第35卷第5期
2016年10月

红外与毫米波学报
J. Infrared Millim. Waves

Vol. 35, No. 5
October, 2016

文章编号: 1001 - 9014(2016)05 - 0534 - 05

DOI:10.11972/j.issn.1001 - 9014.2016.05.005

f_T/f_{max} >150/210 GHz AlGaN/GaN HFETs with regrown n^+-GaN Ohmic contacts by MOCVD

LV Yuan-Jie, FENG Zhi-Hong*, SONG Xu-Bo, ZHANG Zhi-Rong, TAN Xin, GUO Hong-Yu, FANG Yu-Long, ZHOU Xing-Ye, CAI Shu-Jun

(National Key Laboratory of Application Specific Integrated Circuit (ASIC), Hebei Semiconductor Research Institute, Shijiazhuang, 050051, China)

Abstract: Scaled AlGaN/GaN heterostructure field-effect transistors (HFETs) with a high unity current gain cut-off frequency (f_T) and maximum oscillation frequency (f_{max}) were fabricated and characterised on an SiC substrate. In the device, the source-to-drain distance (L_{sd}) was scaled to 600 nm using regrown n^+-GaN Ohmic contacts. In addition, a 60-nm T-shaped gate was fabricated by self-aligned-gate technology. A recorded drain saturation current density (I_{ds}) of 2.0 A/mm at V_{gs} = 2 V and a peak extrinsic transconductance (g_m) of 608 mS/mm were obtained in the scaled AlGaN/GaN HFETs. Moreover, in the devices with a 60-nm T-shaped gate, the maximum values of f_T and f_{max} reached 152 and 219 GHz, respectively.

Key words: AlGaN/GaN, HFET, f_T, f_{max}, regrown Ohmic contacts

PACS: 85.30.De, 71.55.Eq, 85.30.Tv, 78.55.Cr

基于 MOCVD 再生长 n^+ GaN 欧姆接触工艺 f_T/f_{max} >150/210 GHz 的 AlGaN/GaN HFETs 器件研究

吕元杰, 冯志红*, 宋旭波, 张志荣, 谭 鑫, 郭红雨, 房玉龙, 周幸叶, 蔡树军

(河北半导体研究所 专用集成电路国家级重点实验室,河北 石家庄 050051)

摘要:基于 SiC 衬底 AlGaN/GaN 异质结材料研制具有高电流增益截止频率(f_T)和最大振荡频率(f_{max})的 AlGaN/GaN 异质结场效应晶体管(HFETs). 基于 MOCVD 外延 n^+ GaN 欧姆接触工艺实现了器件尺寸的缩小,有效源漏间距(L_{sd})缩小至 600 nm. 此外,采用自对准工艺制备了 60 nm T 型栅. 由于器件尺寸的缩小,在 V_{gs} = 2 V 下,器件最大饱和电流(I_{ds})达到 2.0 A/mm,该值为 AlGaN/GaN HFETs 器件直流测试下的最高值,器件峰值跨导达到 608 mS/mm. 小信号测试表明,器件 f_T 和 f_{max} 最高值分别达到 152 GHz 和 219 GHz.

关 键 词:AlGaN/GaN;异质结场效应晶体管;电流增益截止频率;最大振荡频率;再生长欧姆接触

中图分类号:TN385 **文献标识码**:A

Introduction

Attributed to the unique high breakdown electric field (3.3 MV/cm) combined with a high electron velocity ($v_{peak} \approx 2.5 \times 10^7$ cm/s), GaN-based heterostructure field-effect transistors (HFETs) have attracted significant research attention because of their excellent potential application in high-voltage, and high-power operations in the millimetre-wave frequency range[1-2]. As typical devices, the AlGaN/GaN HFETs, having a high electron mobility and sheet density, have been extensively studied for over twenty years. Nowadays, the performance of AlGaN/GaN HFETs has been greatly improved due to the developments in material growth and device technology[3-4]. AlGaN/GaN HFETs are widely used in solid-state high-power power amplifiers (PA), which have already covered that part of the frequency spectrum

Received date: 2015-00-00, **revised date**: 2016-00-01 **收稿日期**:2015-00-00, **修回日期**:2016-00-01

Foundation items:Supported by the National Natural Science Foundation of China (61306113)

Biography:LV Yuan-Jie (1985-), male, Shandong, China, Ph. D. Research fields focus on GaN-based electronic devices. E-mail: yuanjielv@163.com

* **Corresponding author**:E-mail: ga917vv@163.com

ranging from the L-band to the W-band. Compared with GaAs-based devices, the adoption of AlGaN/GaN HFETs leads to PAs with a higher output power density, greater linearity, and a wider operational bandwidth: these will improve the next generation of high-data-rate phased array radars, communication systems, and active imagers[5].

In recent years, outstanding progress in the frequency performance of AlGaN/GaN HFETs has been achieved. Palacios, *et al.* reported 100nm T-shaped AlGaN/GaN HFETs with a unity current gain cut-off frequency (f_T) of 124 GHz and a maximum oscillation frequency (f_{max}) of 230 GHz[6]. To suppress short-channel effects, a 6-nm-thick AlGaN barrier layer was used by Higashiwaki, *et al.*, and a 55-nm-gate AlGaN/GaN HFET was fabricated[7] with a high f_T of 190 GHz and a f_{max} of 241 GHz at different biases. A 55-nm-gate AlGaN/GaN HFET with a recorded f_T of 225 GHz was reported by Chung, *et al.*, but their device has a low f_{max} of 120 GHz[8]. The same group used recessed source/drain Ohmic contacts and gate-recess technology to reduce parasitic resistances and suppress short-channel effects (SCEs): their AlGaN/GaN HFETs, with a 60nm gate length, realised a recorded f_{max} of 300 GHz [9].

Several complications affect the performance of AlGaN/GaN HFET devices, such as parasitic resistances and capacitances, the nano-T-shaped gate, and SCEs. A combination thereof is needed in high-performance AlGaN/GaN HFETs. Among most of the reported AlGaN/GaN HFETs, conventional Ti/Al-based Ohmic stacks were used, which are considered to run counter to the principles of device scaling. Regrown n^+-GaN Ohmic contacts, which have been widely used in high-frequency (In)AlN/GaN HFETs, can realise not only a low Ohmic resistance, but also a nano-level scale. In this work, regrown n^+-GaN Ohmic contacts were adopted to scale down the source-to-drain distance (L_{sd}). A high-performance, 60nm, T-shaped, AlGaN/GaN HFET was fabricated: when tested it had a recorded direct current (DC) drain current density of 2.0 A/mm at V_{gs} = 2 V and a peak extrinsic transconductance (g_m) of 608 mS/mm. In addition, the maximum values of f_T and f_{max} for the fabricated device reached 152 GHz and 219 GHz at different biases, respectively.

1 Experimental work

In this work, AlGaN/GaN heterostuctures were epitaxially grown on a SiC substrate by metal organic chemical vapour deposition (MOCVD). Epilayers consisted of a 15 nm undoped $Al_{0.28}Ga_{0.72}N$ barrier layer, a 1 nm AlN layer, and a 2 μm undoped GaN buffer layer. Hall effect measurements showed an electron sheet concentration of 1.12×10^{13} cm^{-2} and an electron mobility of 1 990 $cm^2/(V\cdot s)$, resulting in a sheet resistance of 249 Ω/□ at room temperature.

A schematic cross-section of the fabricated AlGaN/GaN HFET is shown in Fig. 1. A 100nm high mesa isolation was firstly etched by a Cl_2/BCl_3 plasma-based dry etching process. Subsequently, the AlGaN/GaN heterostructure was deposited with an SiO_2 mask for n^+-GaN ohmic regrowth by plasma enhanced chemical vapour deposition (PECVD). Using reactive ion etching (RIE), the source and drain regions were patterned. A regrowth well-to-well distance (*i. e.*, $L_{sd\text{-}regrown}$) of 600 nm was defined to reduce the parasitic resistance. Si doped n^+ GaN was regrown by MOCVD, and the doping level was *c.* 3×10^{19} cm^{-3}. The n^+ GaN formed on top of the SiO_2 was lifted off by HF after regrowth. A Ti/Au metal stack was deposited as an Ohmic contact. Using transmission line method (TLM) measurements, the total Ohmic resistance (R_{tot}) was found to be 0.35 Ω · mm. In the analysis, all of the dimensions of the patterns in TLM were confirmed by scanning electron micrograph (SEM). Due to the low Si-doping level, and the damage induced by plasma dry etching, the value of R_{tot} was higher than that reported elsewhere[10]. Using a trilayer photoresist, electron-beam lithography was used to define a 60 nm T-shaped gate which was self-aligned to the n^+-GaN ohmic contacts. The Schottky gate was positioned so as to be in the middle of the source and drain. Finally, a SiN passivation layer was deposited by PECVD and patterned for contact pads using RIE.

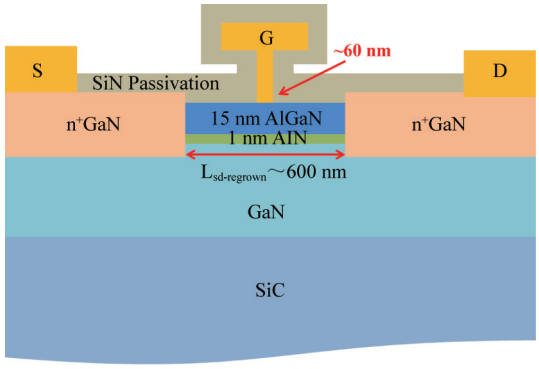

Fig. 1　Schematic cross section of the fabricated AlGaN/GaN HFETs
图 1　AlGaN/GaN HFETs 器件截面示意图

2 Results and Discussion

Using a semiconductor characterisation system, the DC properties of the AlGaN/GaN HFETs with their gate width of 40 μm were measured (Fig. 2). In the output measurements, the drain-source voltage was increased from 0 V to 15 V, in 0.1 V increments, while the gate bias ranged from 2 V to -6 V, in -1 V increments. Testing of the device revealed a recorded maximum drain current density (I_{ds}) of 2.0 A/mm at V_g = 2 V in DC mode. The value of on-resistance (R_{on}) for the fabricated device was found to be just 0.94 Ω · mm at V_{gs} = 1 V. The transfer characteristics of the fabricated AlGaN/GaN HFET at V_{ds} = 6 V are shown in Fig. 2(b). A peak extrinsic transconductance (g_m) of 608 mS/mm was found. To the best of our knowledge, the I_{ds} of 2.0 A/mm is a recorded value (to date) for AlGaN/GaN HFETs in DC mode. The high value of I_{ds} is mainly due

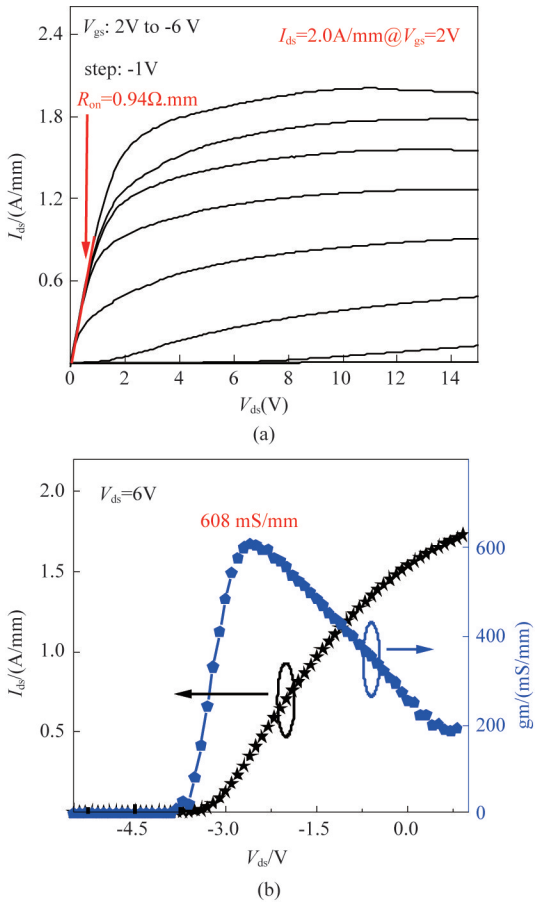

Fig. 2 DC output (a) and transfer characteristics (b) of the fabricated AlGaN/GaN HFETs

图 2 AlGaN/GaN HFETs 器件直流输出(a)和转移特性曲线(b)

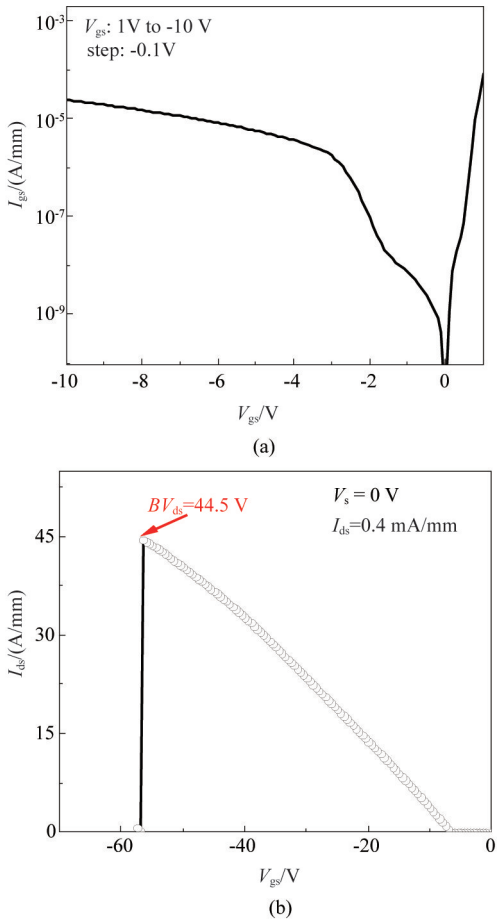

Fig. 3 The I_{gs}-V_{gs} characteristics (a) and V_{ds}-V_{gs} breakdown sweeps of the fabricated AlGaN/GaN HFETs

图 3 AlGaN/GaN HFETs 器件 I_{gs}-V_{gs} 特性(a)和 V_{ds}-V_{gs} 特性曲线(b)

to the effective device scaling, resulting in a low R_{on}. Moreover, the SiN passivation can compensate the surface states and increase the 2DEG density in the channel, which further enhanced the drain current density. In addition, as seen from Fig. 2 (a), the AlGaN/GaN HFET showed good pinch-off characteristics. No thermal effect was observed due the high thermal conductivity of the SiC substrate. However, obvious SCEs were seen, as evinced by the increased output conductance. This was mainly due to the low aspect ratio (L_g/d, where d is the barrier thickness). Moreover, the increase in 2DEG density in the access region after SiN passivation also enhanced the SCEs.

The gate leakage current characteristics of the fabricated AlGaN/GaN HFETs were measured, and the device revealed a low gate leakage current of 2.5×10^{-5} A/mm even at V_g = -10 V, as shown in Fig. 3(a). The V_{ds} versus V_{gs} breakdown characteristics with I_{ds} fixed at 0.2 mA/mm were also measured (Fig. 3(b)). Using the constant drain current injection method, the off-state breakdown voltage BV_{ds} was measured as being 44.5 V. The shoulder at V_g of -7 V in the breakdown curve corresponded to the onset of flow of the gate leakage current. From the V_{ds} versus V_{gs} curve, the catastrophic gate-to-drain breakdown voltage can be extracted: the plotting revealed this to be 101 V. Corresponding to the above values, the gate-to-drain breakdown field was calculated as 3.36 MV/cm, which approached the critical field value for GaN (3.4 MV/cm), which indicated a good crystal quality in this AlGaN/GaN heterostucture on its SiC substrate. Of course, ignoring the n^+ GaN in the gate-to-drain region may have added to the calculated value of the gate-to-drain breakdown field.

Table 1 Main model parameters at different biases

表 1 不同偏置电压下主要的模型参数

	V_{gs} = -2.8 V, V_{ds} = 6 V	V_{gs} = -2.8 V, V_{ds} = 14 V
g_m/(mS/mm)	777	602
g_{ds}/(mS/mm)	81	40.7
C_{gd}/(fF/mm)	108	70

The small-signal RF measurements of the AlGaN/GaN HFETs were carried out over the range of 100 MHz to 50 GHz in increments of 0.05 GHz using a vector network analyser. With on-wafer open/short calibration structures, the parasitic pad inductances and capacitances were de-embedded from the measured S-parameters[11]. The values of f_T and f_{max} can be obtained by extrapolating the current gain $|H_{21}|^2$ and the maximum available gain (MAG) derived from measured S-parame-

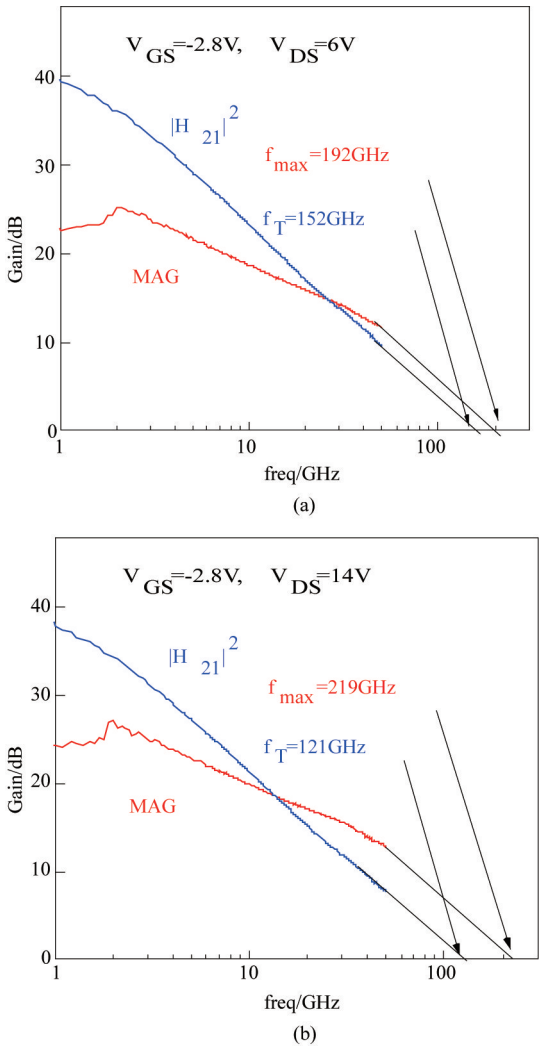

Fig. 4　Small signal RF performance of the prepared AlGaN/GaN HFETs corresponding to the peak f_T (a) and f_{max} (b)

图 4　AlGaN/GaN HFETs 器件中对应 f_T (a) 和 f_{max} (b) 最高值的射频小信号曲线

ters by -20 dB/dec. Figures 4(a) and (b) characterize the behavior of $|H_{21}|^2$ and MAG when plotted against frequency at different biases corresponding to the peak values of f_T and f_{max}, respectively. A peak f_T of 152 GHz was obtained at a V_gs of -2.8 V and a V_{ds} of 6 V, combined with an f_{max} value of 192 GHz. In addition, a peak f_{max} of 219 GHz was obtained at a V_{gs} of -2.8 V and a V_{ds} of 14 V, but the value of f_T dropped to 121 GHz. Table 1 lists the main model parameters at V_{ds} of 6 V and 14 V, respectively. The intrinsic transconductance (g_m) decreased significantly from 777 mS/mm to 602 mS/mm, with increasing drain bias, resulting in a decrease in f_T. However, the output conductance (g_{ds}) decreased from 81 to 40.7 mS/mm, indicating that the SCE was weakened. This can also be seen from the output characteristics. As a result, the value of f_{max} increased with increasing drain bias.

As shown in Fig. 5, several results from the testing of AlGaN/GaN HFETs from different groups are summarized[6-9,12-17]. Many reported AlGaN/GaN HFETs exhibit a low value of $\sqrt{f_T \cdot f_{max}}$ and often one less than 150 GHz. The value of $\sqrt{f_T \cdot f_{max}}$ for these fabricated AlGaN/GaN HFETs was about 170 GHz, which was close to the best yet achieved of 183 GHz[19]. The values of f_T and f_{max} were mainly affected by gate length, parasitic resistance, and parasitic capacitance. Moreover, the output conductance (g_{ds}), as related to the SCEs, exerted a significant influence on the value of f_{max}. To improve the frequency characteristics even more, a thinner barrier layer, and a thinner gate recess would be needed to suppress the SCEs.

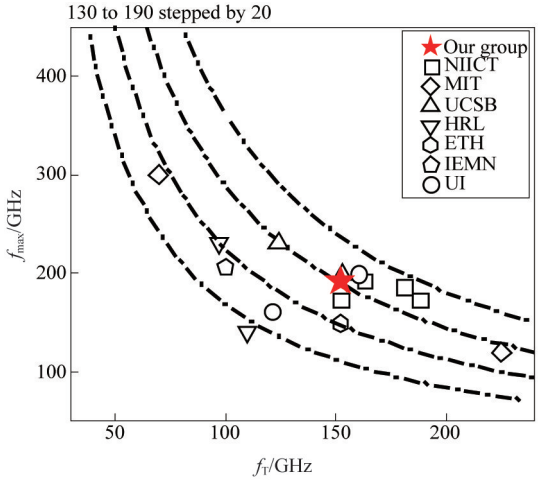

Fig. 5　Comparison of measured f_T and f_{max} in AlGaN/GaN HFETs from different groups

图 5　国内外 AlGaN/GaN HFETs 器件 f_T 和 f_{max} 频率特性对比图

3　Conclusions

In summary, AlGaN/GaN HFETs with high values of f_T and f_{max} were fabricated and characterized on a SiC substrate. To reduce the parasitical resistance, including R_d, R_s, and R_i, the source-to-drain distance (L_{sd}) was scaled to 600 nm using regrown n^+-GaN Ohmic contacts by MOCVD. In addition, a 60-nm T-shaped gate was fabricated by self-aligned-gate technology and located in the middle of the source and drain contacts. Due to the scaled source-to-drain distance, the AlGaN/GaN HFET showed a recorded high I_{ds} of 2.0 A/mm at V_{gs} = 2 V and a peak g_m of 608 mS/mm. On-wafer small-signal RF measurements indicated that the peak values of f_T and f_{max} for the device were 152 GHz and 219 GHz, respectively.

References

[1] Shen L, Palacios T, Poblenz C, *et al*. Unpassivated High Power Deeply Recessed GaN HEMTs With Fluorine-Plasma Surface Treatment [J]. *IEEE Electron Device Letters*, 2006, **27**: 214 - 216.

[2] Micovic M, Kurdoghlian A, Shinohara K, *et al*. W-band GaN MMIC with 842 mW output power at 88 GHz. *IEEE IMS*, 2010, Anaheim, CA: 237 - 239.

(下转第 568 页)

environment of green fluorescent protein[J]. *Biophysical Journal*, 2002, **83**(6):3589-3595.
[3] LACAITA A L, FRANCESE P A, COVA S D, *et al*. Single-photon optical-time-domain reflectometer at 1.3 micron with 5-cm resolution and high sensitivity[J]. *Optics Letters*, 1993, **18**(13):1110-1112.
[4] ERAERDS P, LEGRE M, ZHANGJ, *et al*. Photon counting OTDR: advantanges and limitations[J]. *Journal of Lightwave Technology*, 2010, **28**(6):952-964.
[5] ZBINDEN H, BECHMANN-PASQUINUCCI H, GISIN N, *et al*. Quantum cryptography[J]. *Applied Physics B*, 1998, **67**(6):743-748.
[6] ZHANG J, ERAERDS P, WANLENTA N, *et al*. 2.23 GHz gating InGaAs/InP single-photon avalanche diode for quantum key distribution[J]. *Proc. SPIE*, 2010, **7681**: 76810Z.
[7] PENG C, ZHANG J, YANG D, *et al*. Experiemental long-distance decoy-state quantum key distribution based on polarization encoding[J]. *Physical Review Letters*, 2007, **98**(1):010505.
[8] CHEN J, WU G, XU L, *et al*. Stable quantum key distribution with active polarization control based on time-division multiplexing[J]. *New Journal of Physics*, 2009, **11**(6): 065004.
[9] NAMBU Y, TAKAHASHI S, YOSHINO K, *et al*. Efficient and low-noise single-photon avalanche photodiode for 1.244-GHz clocked quantum key distribution[J]. *Optics Express*, 2011, **19**(21):20531-20541.
[10] REN M, GU X, LIANG Y, *et al*. Laser ranging at 1550 nm with 1GHz sine-wave gated InGaAs/InP APD single-photon detector[J]. *Optics Express*, 2011, **19**(14): 13497.
[11] YANG Fang, ZHANG Xin, HE Yan, *et al*. Laser ranging system based on high speed pseudorandom modulation and photon counting techniques[J]. *Chinese Journal of Lasers* (杨芳, 张鑫, 贺岩,等. 基于高速伪随机码调制和光子计数激光测距技术. **中国激光**), 2013, **40**(2):184-188.
[12] CHEN Xiu-Liang, 1550nm single-photon detection and its applications[D]. East China Normal University (陈修亮. 1 550 nm 单光子探测极其应用研究. 华东师范大学) 2006.
[13] YUAN Z L, KARDYNAL B E, SHARPE A W, *et al*. High speed single photon detection in the near infrared[J]. *Applied Physics Letters*, 2007, **91**(4):041114.
[14] LI Yong-Fu, LIU Jun-Liang, WANG Qing-Pu, *et al*. Avalanche characterization of high speed single-photon detector based on InGaAs/InP APD[J]. *J. Infrared Millim. Waves* (李永富, 刘俊良, 王青圃,等. 基于 InGaAs/InP 雪崩二极管的高速单光子探测器雪崩特性研究. **红外与毫米波学报**), 2015, **34**(4):427-431.
[15] ZHENG Li-Xia, WU Jin, ZHANG Xiu-Chuan, *et al*. Sensing detection and quenching method for InGaAs single-photon detector[J]. *Acta Phys. Sin.* (郑丽霞,吴金,张秀川等. InGaAs 单光子探测器传感检测与淬灭方式. **物理学报**), 2014, **63**(10):104216.
[16] NAMEKATA N, SASAMORI S, INOUE S. 800 MHz single-photon detection at 1550-nm using an InGaAs/InP avalanche photodiode operated with a sine wave gating[J]. *Optics Express*, 2006, **14**(21):10043-10049.
[17] ZHANG J, THEW R, BARREIRO C, *et al*. Practical fast gate rate InGaAs/InP single-photon avalanche photodiodes[J]. *Applied Physics Letters*, 2009, **95**(9):091103.
[18] WU G, ZHOU C, CHEN X, *et al*. High performance of gated-mode single-photon detector at 1.55 um[J]. *Optics Communications*, 2006, **265**(2006):126-131.

(上接537页)

[3] Kuzmík J. Power electronics on InAlN/(In)GaN: Prospect for a record performance[J]. *IEEE Electron Device Letters*, 2001, **22**: 510-512.
[4] Sun H, Alt A R, Benedickter H, *et al*. 205-GHz (Al,In)N/GaN HEMTs[J]. *IEEE Electron Device Letters*, 2010, **31**:293-295.
[5] Brown A, Brown K, Chen J, *et al*. W-band GaN power amplifier MMICs[C]. *IEEE MTT-S International*, 2011, Baltimore, MD:1-4.
[6] Palacios T, Dora Y, Chakraborty A, *et al*. Optimization of AlGaN/GaN HEMTs for high frequency operation[J]. *phys. stat. sol.* (*a*), 2006, **203**: 1845-1850.
[7] Higashiwaki M, Mimura T, Matsui T. AlGaN/GaN Heterostructure Field-Effect Transistors on 4H-SiC Substrates with Current-Gain Cutoff Frequency of 190 GHz[J]. *Applied Physics Express*, 2008, **1**: 021103-(1-3).
[8] Chung J W, Hoke W E, Chumbes E M, *et al*. Advanced gate technologies for state-of-the-art f_T in AlGaN/GaN HEMTs[C]. *IEDM Tech. Dig*, 2010, **30**:1-4.
[9] Chung J W, Hoke W E, Chumbes E M, *et al*. AlGaNGaN HEMT with 300-GHz f_{max}[J]. *IEEE Electron Device Letters*, 2010, **31**: 195-197.
[10] Guo H Y, Lv Y J, Gu G D, *et al*. High-Frequency AlGaN/GaN High-Electron-Mobility Transistors with Regrown Ohmic Contacts by Metal-Organic Chemical Vapor Deposition[J]. *Chin. Physics Letter*, 2015, **32**: 118501-(1-3).
[11] Chen G, Kumar V, Schwindt R S, *et al*. Low Gate Bias Model Extraction Technique for AlGaN/GaN HEMTs[J]. *IEEE Trans Micro Theory Tech*, 2006, **54**: 2949-2953.
[12] Higashiwaki M, Matsui T. AlGaN/GaN Heterostructure Field-Effect Transistors with Current Gain Cut-off Frequency of 152 GHz on Sapphire Substrates[J]. *Japanese Journal of Applied Physics*. 2005, **44**: 475-478.
[13] Higashiwaki M, Mimura T, Matsui T. 30-nm-Gate AlGaN/GaN Heterostructure Field-Effect Transistors with a Current-Gain Cutoff Frequency of 181 GHz[J]. *Japanese Journal of Applied Physics*, 2006, **45**: 1111-1113.
[14] Palacios T, Chakraborty A, Heikman S, *et al*. AlGaN/GaN high electron mobility transistors with InGaN back-barriers[J]. *IEEE Electron Device Letters*, 2006, **27**: 13-15.
[15] Brown D F, A Williams, Shinohara K, *et al*. W-band power performance of AlGaN/GaN DHFETs with regrown n+ GaN ohmic contacts by MBE[C]. *IEEE Electron Devices Meeting* (*IEDM*), 2011, Washington, DC: 461-464.
[16] Kim D, Kumar V, Lee J, *et al*. Recessed 70-nm Gate-Length AlGaN/GaN HEMTs Fabricated Using an Dielectric Layer[J]. *IEEE Electron Device Letters*, 2009, **30**: 913-915.
[17] Bouzid-Driad S, Maher H, Defrance N, *et al*. AlGaN/GaN HEMTs on Silicon Substrate With 206-GHz[J]. *IEEE Electron Device Letters*, 2013, **34**:36-38.